scientific reports

Check for updates

OPEN

Head injury risk prediction for vulnerable road users based on Chinese adult male head data

Ying Lu[1]✉, Jun Bai[1], Yufa Liu[1,3] & Yu Shu[2]

Prediction of injuries to vulnerable road users (VRUs) during the head-ground collision phase has been a long-standing challenges in accident modeling. This study aims to reveal the severity of head injury in vehicle-VRU collision (VVC) accidents and quantify the relationship between the head-ground collision (HGC) velocity and the injury levels of brain tissue with local human attributes. First, a finite element head model with Chinese human attributes was constructed and verified. The simulation model of the HGC was subsequently established and verified by comparison with the Nahum Experiment, Yoganandan experiment, and head-fall-to-ground (HFOG) experiments. Finally, regression models for the relationships between the HGC velocity and injury parameters of the brain tissue were constructed, and the optimal cutoff value of the HGC velocity was determined. Based on the results of the VVC accident reconstruction and case studies, these regression models and the cutoff value of the HGC velocity can accurately determine the severity of head injuries in pedestrians.

Keywords Head-ground collision, Finite element simulation, Head injuries, Vehicle-vulnerable road user accident

List of symbols

λ_i	Scaling factor on the corresponding dimension
W	The width of the head
G_0	Short-term shear modulus
β	Parameters of viscoelastic behavior of materials
ρ	Density
E	Elastic modulus
σ_f	Fracture stress
K	Bulk modulus
αl	Coefficient of linear expansion
g	Gravitational acceleration
v0	Initial speed
σ_{DN}	The stress of cerebrum
σ_{XN}	The stress of cerebellum
ICP_{QM}	Quadratic model of the ICP
CR_{QM}	Quadratic model of the cerebrum
BS_{QM}	Quadratic model of the brainstem
CL_{QM}	Quadratic model of the cerebellum
C	The circumference of the head
L	The head length
G_∞	Long-term shear modulus
t	Time duration
v	Poisson's ratio
Y_o	Yield stress
ε	Strain of failure
λ	Thermal conductivity
h	The free-fall height
V	Head-ground collision velocity

[1]School of Automotive and Traffic Engineering, Jiangsu University, Zhenjiang 212013, China. [2]Fourth People's Hospital of Zhenjiang, Zhenjiang 212013, China. [3]Present address: School of Automotive Engineering, Changzhou Vocational College of Technology, Changzhou 213161, China. ✉email: luying@ujs.edu.cn

P0	Intracranial pressure
σ_{NG}	The stress of brainstem
ICP_{LM}	Linear model of the ICP
CR_{LM}	Linear model of the cerebrum
BS_{LM}	Linear model of the brainstem
CL_{LM}	Linear model of the cerebellum

According to the World Health Organization, approximately 1.35 million people die in road traffic accidents every year worldwide[1,2]. It has also been reported that more than 50% of the dead are vulnerable road users (VRUs), including pedestrians, cyclists and riders of powered two-wheeler vehicles. In China, the disability and death of VRUs caused by vehicle-VRU collision (VVC) accidents are increasing yearly. In 2022, approximately 60,000 people died from road traffic accidents in China, of which the total number of VRU deaths was approximately 16,300, accounting for 25% of the annual road accident fatalities[3].

Generally, the whole process of VVC includes two phases: the first phase involves the VRU being hit by the vehicle; the second phase involves the VRU falling onto the ground after separating from the vehicle, sliding along the ground, and tumbling to rest[4]. Head injuries, which are the most fatal factors to VRUs, may result from both the first and the second phases[5]. It has been reported that 95% of the impact velocities of VVC accidents are between 25 and 55 km/h[6]. Under these circumstances, the second phase may cause more severe head injuries than the collision in the first phase[7,8]. Additionally, the impact area of the vehicles, including the engine hood and windshield, has been carefully designed to meet safety criteria, such as the European Enhanced Vehicle-safety Committee Working Group 17 (EEVC WG 17) test procedures[9]. Hence, significant progress has been made in reducing VRU injury in the first phase. However, in the second phase, the ground material has almost no damping when the head impacts the ground. This may lead to a severe head injury[10]. Hence, this study focuses on the head-ground collision (HGC) during the second phase.

Much research has been conducted on the biomechanics of head injuries[11] to reduce fatal injuries to pedestrian. Due to its high efficiency and adjustment flexibility, the multibody (MB) model[8] is popular in accident reconstruction and injury analysis. However, the MB model cannot obtain the specific injury parameters of brain tissues. The finite element (FE) model[12] is another widely-used method for head injury evaluation and can be used to assess brain-tissue-level damage. With the development of computer technology, the FE head model has been significantly improved enabling researchers to conduct more accurate investigations on the biomechanical response of head injury[13]. Marjoux et al.[14] presented the Louis Pasteur University (ULP) human head FE model, which based on actual accident cases has a better ability to predict moderate-to-severe craniocerebral injury than the head injury criteria (HIC) and head impact force (HIP) injury metrics. Fredriksson et al.[15] conducted FE simulations using the Polar II pedestrian dummy model to investigate the potential of active, passive, and integrated safety systems to reduce pedestrian upper body loads in the first crash. Tamura et al.[16] used the Ford Explorer vehicle FE model and the Total Human Model for Safety (THUMS) FE pedestrian model for crash studies. They reported that translational and rotational accelerations were significantly correlated with the severity of intracranial tissue deformation. Wei et al.[17] developed an FE model of an electric scooter (ES) dummy based on the hybrid III FE model to evaluate the HGC conditions and the effects of helmets on head protection during typical ES falls.

In the field of predicting head injuries in VRUs involving VVCs, the use of data-driven methods is the major methodological approach. The used data can be classified into three main types. The first is a third-party-collected accident database, such as the national automotive sampling system crashworthiness data system (NASS CDS) in the USA, the German In-Depth Accident Study (GIDAS), and the China In-Depth Study of Traffic Accidents (CIDAS). The second one is local accident cases collected by the researchers themselves, which commonly involve accident reconstruction. The third is the simulation data, which can be generated by use MB and FE models. With these data, the head injury prediction model can be obtained by using regression analysis, machine learning, and deep learning. Marc et al.[18] reconstructed and analyzed head injury scenarios of VRUs in 27 cases. Liu et al.[19] developed a prediction model using an artificial neural network based on data from 218 accidents. Hiromichi et al.[20] reconstructed a head finite element model using volunteer data, and simulation analysis revealed that collision speed was the most significant factor affecting the von Mises stress. Shi et al.[21] reconstructed 10 VRU accident cases that included video footage and selected seven key parameters as criteria, successfully predicting at least 75% of the accidents.

However, the current studies on head injury analysis and prediction in VVC still exhibit some limitations. First, most actual accident databases provide only the overall level of damage to the head, such as Abbreviated Injury Scale (AIS) levels and the Injury Severity Score (ISS) for the head, which cannot be used in brain-tissue-specific injury prediction. Second, most existing FE head models, and in particular those used in commercial software, are usually based on human data from Western countries. For example, the popular FE model, THUMS, developed by Toyota Motor Corporation is based on data from the Visible Human Project in the USA[22]. This class of FE head models typically needs to be modified to meet the national conditions of each country. Third, although some researchers have provided some insight into the extent of damage to brain issues, few studies have specifically analyzed the stress injury of each main brain tissue. Fourth, to the best of our knowledge, few studies have quantified the relationship between the degree of injury to brain tissues and the velocity of HGC. For these reasons, this study intended to develop a head FE model with Chinese human attributes and use it to study head-ground contact injuries in human-vehicle collisions.

The primary aim of this study was to construct models relating the velocity of HGC and the degree of injury to human brain tissues. First, an FE head model of 50th-percentile Chinese adult males was constructed and validated. Next, a regression model for the relationship between the HGC velocity and injury parameters of the brain, including intracranial pressure (ICP) and brain-tissue stress, was established. Then, the optimal cutoff

value of the HGC velocity was determined. Finally, the validity of the regression models was examined using accident reconstruction.

Head FE modeling

Head FE model in China

Currently, the most widely used human FE models in China, such as the THUMS and Global Human Body Model Consortium (GHBMC) models, were developed based on the human data in the USA. The dynamic response characteristics of human finite element models under collision loads are also determined on the basis of American cadaver test data. However, there are large differences between the Chinese and American human bodies in terms of both external physical signs (e.g., height, weight, muscle density, mass distribution) and internal characteristics (dynamic response, biomechanics). For example, compared with medium-sized men in the United States, the corresponding male dummies in China must be 3.48% shorter and 11.89% lighter. The upper arms of Chinese medium-sized men are 4.14% shorter than those of medium-sized men in the United States, and the knee height is 12% shorter in the sitting position[23,24]. The difference in biomechanical properties is also highly significant and directly affects the human tolerance limit and the evaluation index and limit of the test dummy. Hence, some Chinese researchers have proposed different methods to develop FE models that are more consistent with the characteristics of the Chinese human body. In this study, we focus on methods for constructing Chinese human head models.

The *scaling method*, that is, scaling the existing mature FE dummy models, as shown in Fig. 1, is one the main methods for the development of FE models. This approach not only reduces the development cycle and cost of the dummy model but also ensures the biological realism of the dummy. When dealing with the scaling factor of adults, it is often assumed that the density and stiffness of biological tissues and materials of adults are the same; thus, the geometric scaling factor is an important parameter in the process of obtaining the Chinese adult dummy model using the scaling method.

Two scaling methods are commonly used for the dummy head model. The first is the uniform scaling method; that is, the scaling coefficients in the X, Y and Z directions, denoted by λ_x, λ_y, λ_z respectively, are equal in the local coordinate system of the dummy head, as shown in Fig. 1b. The specific head scaling coefficient is given as follows:

$$\lambda_x = \lambda_y = \lambda_z = \frac{(\boldsymbol{C_1} + \boldsymbol{W_1} + \boldsymbol{L_1})}{(\boldsymbol{C_0} + \boldsymbol{W_0} + \boldsymbol{L_0})} \tag{1}$$

$$\lambda_{\mathrm{m}} = \lambda_x \cdot \lambda_y \cdot \lambda_z \tag{2}$$

where C is the circumference of the head, W is the width of the head (Y direction); L is the head length (X direction); λ_{m} is the scaling factor for the mass of the head; Subscript 1 indicates Chinese human body parameters; and subscript 0 indicates American human body parameters.

The second scaling method is the nonuniform scaling method, as shown in Fig. 1c, for which the scaling coefficients are given by:

$$\lambda_x = L_1/L_0 \tag{3}$$

$$\lambda_y = W_1/W_0 \tag{4}$$

$$\lambda_z = \lambda_{\mathrm{m}}/(\lambda_x \cdot \lambda_y) \tag{5}$$

The width of the human head in China is basically the same as that in the US while, the difference between the Chinese and American head lengths is large. If the scaling method of the uniform coefficient is adopted, the contour line of the obtained dummy head model in the sagittal plane and the coronal plane is significantly different from the geometric parameters of the head of the Chinese human body. Hence, it is suggested that the nonuniform scaling method should be used to obtain the Chinese dummy head model.

In addition to geometric size, brain structure differences between Chinese and Western population cohorts also exist. Compared with the Western population, the Chinese population presented greater structural features

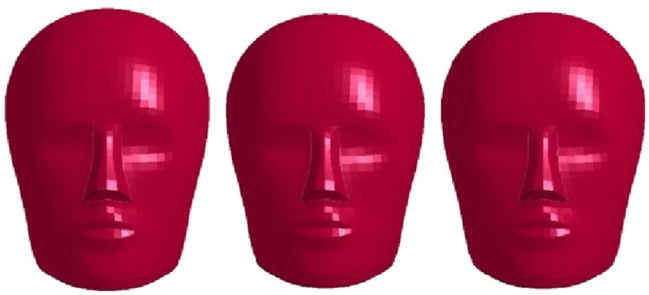

Fig. 1. Chinese head FE model constructed via the scaling method. (**a**) Original dummy (e.g., Hybrid III), (**b**) uniform scaling, (**c**) nonuniform scaling.

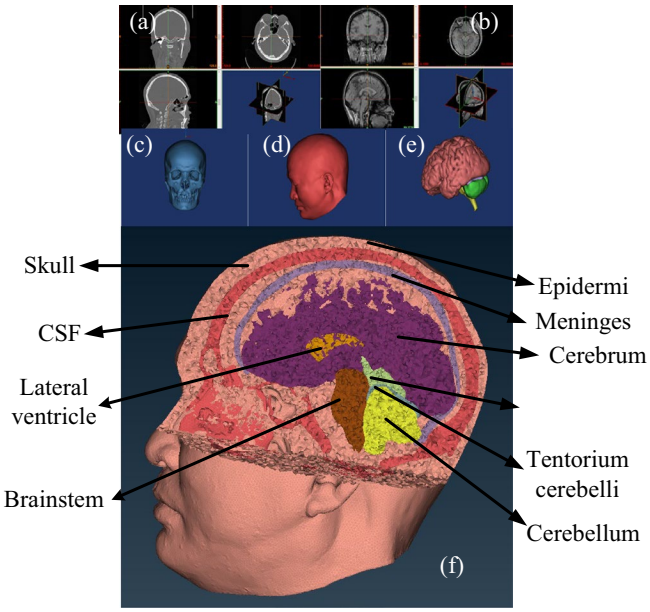

Fig. 2. Construction of the head FE model of a 50th-percentile adult male: (**a**) CT scan data, (**b**) MRI scan data, (**c**) skull geometry model, (**d**) scalp geometry model, (**e**) brain tissue geometry model, (**f**) head FE model.

Components	Min	Max
Skull	226	3071
Lateral ventricle	0	134
Brainstem	114	657
Meninges	0	555
Cerebrum	114	657
Cerebellum	114	657
Tentorium cerebelli	40	261
Third ventricle	40	261

Table 1. Gray value thresholds for skull and intracranial tissues.

in the temporal lobe and cingulate gyrus, and smaller features in the frontal lobe and parietal lobe. Because most business FE models provide only the synthetic acceleration of the head center of mass, investigations of the injury level of Chinese population based only on these FE models are insufficient.

Therefore, there is still a need for the generation of high biofidelity human head models to comprehensively understand injury mechanisms. In this study, we constructed a FE human head model based on the basis of computed tomography (CT) and magnetic resonance imaging (MRI) data from Chinese adult males. This model can provide some insight into the extent of injury to various brain issues.

Construction of the FE head model

We developed an FE head model of a 50th-percentile Chinese adult male volunteer whose height and weight were 169.25 cm and 64.5 kg, respectively. Figure 2a, b shows the head data obtained from the CT and MRI scans, respectively.

We imported the CT and MRI data into the MIMICS (https://www.mimics.com) software and adjusted the contrast values (that is, gray value thresholds, as shown in Table 1). Then, geometric models of the skull, scalp, and brain tissues were generated, as shown in Fig. 2c–e.

ANSA (www.beta-cae.com) software was used to mesh the head geometry model to generate the FE head model. Table 2 shows the material properties and constitutive model of the FE head model. The material properties of the brain tissues (that is, the cerebrum, brainstem, and cerebellum) and cerebrospinal fluid (CSF) are assumed to be linear, isotropic and viscoelastic. The shear characteristic of viscoelastic behavior is expressed as follows:

$$G(t) = G_\infty + (G_0 - G_\infty)e^{-\beta t} \tag{6}$$

where G_0 and G_∞ denote the short-term and long-term shear moduli, respectively, β is a decay constant, and t is the time duration.

Components	Constitutive model	Material properties
Cortical Bone	Elastoplastic	$\rho = 2100\ kg/m^3$, v = 0.26, E = 15.1 GPa, $Y_o = 145$ MPa$\sigma_f = 90$ MPa, $\varepsilon = 0.008$
Cancellous bone	Elastoplastic	$\rho = 1200\ kg/m^3$, v = 0.31, E = 4.64 GPa, $Y_o = 28$ MPa, $\sigma_f = 35$ MPa, $\varepsilon = 0.008$
Lateral ventricle	Elastic	$\rho = 1200\ kg/m^3$, v = 0.45, E = 31.5 MPa
Epidermis	Elastic	$\rho = 1060\ kg/m^3$, v = 0.45, E = 16.8 MPa
Meninges	Elastic	$\rho = 1200\ kg/m^3$, v = 0.42, E = 11.4 MPa
Brainstem	Viscoelastic	$\rho = 1200\ kg/m^3$, v = 0.4999997, E = 4 kPa, K = 2.19 GPa,$G_0 = 22.5$ kPa, $G_\infty = 4.5$ kPa, $\beta = 80\ s^{-1}$
erebrum	Viscoelastic	$\rho = 1060\ kg/m^3$, v = 0.4999997, E = 4 kPa, K = 2.19 GPa, $G_0 = 10.0$ kPa, $G_\infty = 2.5$ kPa, $\beta = 80\ s^{-1}$
Cerebellum	Viscoelastic	$\rho = 1060\ kg/m^3$, v = 0.4999997, E = 4 kPa, K = 2.19 GPa, $G_0 = 10.0$ kPa, $G_\infty = 2.0$ kPa, $\beta = 80\ s^{-1}$
Tentorium cerebelli	Elastic	$\rho = 1200\ kg/m^3$, v = 0.45, E = 31.4 MPa
Third ventricle	Elastic	$\rho = 1200\ kg/m^3$, v = 0.31, E = 31.5 MPa
CSF	Viscoelastic	$\rho = 1000\ kg/m^3$, v = 0.499999, E = 1 kPa, K = 2.19 GPa, $G_0 = 1.0$ kPa, $G_\infty = 0.9$ kPa, $\beta = 80\ s^{-1}$

Table 2. Material property parameters of the FE head model. ρ: density; v: Poisson's ratio; E: elastic modulus; Y_o: yield stress; σ_f: fracture stress; ε: strain at failure; K: bulk modulus.

Consequently, the FE head model is shown in Fig. 2f. It included the skull (cortical bone and cancellous bone), lateral ventricles, brainstem, scalp, pia mater, brain, cerebellum, tentorium, third ventricle, and CSF as shown in Table 3. The total mass of the FE head model is approximately 4.95 kg.

Verification of the FE head model via the Nahum experiment

The cadaveric intracranial pressure (ICP) experiment conducted by Nahum et al.[25] (Experiment 37) has been widely used to validate the biofidelity of the FE head model. Therefore, in this study, we also compared the simulation results of the FE head model with the experimental curves of Nahum Experiment 37. To be consistent with Nahum Experiment 37, in the simulation test, a rigid cylinder impactor with a mass of 5.59 kg was used to impact the frontal bone of the head at 9.49 m/s, as shown in Fig. 3a. The horizontal plane was oriented at 45 degrees to the Frankfort plane. The simulation time was set to 8 ms, and the head was constrained to prevent rotational acceleration.

Figure 3b shows the contact force comparison between the simulation and experiment results. We observed that the experimental peak is 6953 N, and the simulated peak value was 6941 N. The difference in the peak value time occurrence (PVTO) was − 0.6 ms, and the peak percentage difference (PPD) was − 0.17%. Hence, the contact force curves of the simulation and experiment are in good agreement.

Figure 3c–f show the extracted experimental and simulation curves for the impact side pressure, offset side pressure, parietal bone pressure, and occipital bone pressure, respectively.

Figure 4a, b depict the PPD and the difference in PVTO between the curves of the simulation test and the Nahum experiment. We observed that the difference in PVTOs was less than 0.6 ms. The PVTO of the experimental and simulated curves was similar. On the other hand, the PPDs of the impact side pressure and parietal bone pressure agree well with those of the Nahum experiment. Although the PPD values of offset-side pressure and occipital pressure are slightly higher than the experimental values, the error range does not exceed 20%, which is acceptable[26]. Hence, the results of the simulation test and those reported in the Nahum experiment are consistent. Based on the above analysis, we determine that the FE head model is reliable and can be used in subsequent studies.

Validation of experimental data from Yoganandan's experiment

Yoganandan's experiment is used to study the dynamic biomechanical response and injury of a person under the condition of head-to-ground collision[27]. We conducted a simulation test according to Yoganandan's experimental description, as shown in Fig. 5. In the simulation, the head finite element model was placed on the side, and the buffer gasket was fixed horizontally, so that the head model fell at speeds of 3.5, 4.9 and 6 m/s collided with the buffer gasket, and the corresponding contact force curves were obtained, which were compared to the Yoganandan's experimental curves and analyzed. The simulation time was set to 10 ms.

The contact force between the side area of the head and the plate was measured. Figure 6 shows the experimental and simulated results of the contact force of the head model when it falls at different speeds.

Figure 6 shows that the simulation results are consistent with the experimental curve both for the peak value and for the trend of the curve. When the head finite element model falls at different speeds, the peak contact force increases with increasing velocity, and the PVTOs at speeds of 3.5, 4.9 and 6 m/s are 0.1, 0.2 and 0.3 ms, respectively. The PPDs at the speeds of 3.5, 4.9 and 6 m/s are − 7.86%, − 0.13% and − 6.9%, respectively. The contact force peaks and PVTO are close, and all of the PPDs are within 10%, verifying the effectiveness of the model.

HGC simulation and verification

Construction of the HGC simulation model

Before conducting the HGC simulation model, we established the FE model of the ground. Table 4 shows the material property parameters of the ground. Figure 7a shows the FE model of the ground. Then, we integrated

Brain tissue structure	Number of grids	Corresponding graph
Skull	950317	
Lateral ventricle	29275	
Brainstem	66117	
Scalp and cerebrospinal fluid	2694802	
Pia mater	740514	
Brain	860224	
Cerebellum	256902	
Tentorium cerebelli	55541	
Third ventricle	24342	

Table 3. The tissues of each part of the head finite element model.

the FE head and ground models in the ABAQUS (www.goengineer.com/abaqus) software to create the HGC simulation model, as shown in Fig. 7b.

Validation of the HGC simulation model from the perspective of HGC acceleration

Although our FE head model has been validated, the contact between the FE ground and FE head models still needs to be examined, that is, the HGC simulation model needs to be validated.

According to the Calibration Specification for the Anthropomorphic Test Device of Vehicle Frontal Impact Test (JJF 1803-2020) Chinese standard, the hybrid dummy is hung, the lowest point of the dummy's forehead is 12.7 mm below the lowest point of the dummy's nose, and the head of the dummy should fall freely and hit the impact surface, as shown in Fig. 8.

Referring to this Chinese standard, we conduct an experiment to validate the HGC simulation model from the perspective of HGC acceleration. The main factors affecting HGC acceleration are the head mass, head contour, center of mass, and facial skin[28]. Therefore, we used the skull geometry model in Section "Head FE modeling" and 3D printed it to obtain a skull physical model (SPM), which guaranteed that the head contours were consistent with those of the FE model. A silicone human face was added to the SPM to ensure that the mechanical properties were similar to those of the skin. The interior of the head physical model (HPM) was filled with rubber to ensure that it had a consistent mass and a similar center of mass as the FE head model.

The MPA1052A-2000 acceleration sensor was then fixed at the center of mass of the HPM and connected to the GPDAS-8 data acquisition device, as shown in Fig. 9a. The data acquisition software was installed on a Shenzhou Ares TX8-CU5DS laptop, as shown in Fig. 9b. Finally, the GPDAS-8 data acquisition device was connected to the laptop, as shown in Fig. 9c.

The test scenario is shown in Fig. 9d. We suspended the HPM on a rack according to Chinese standards JJF 1803-2020, with the center symmetry plane of the HPM perpendicular to the ground. Then, the HPM was released with zero initial velocity, so that it fell in a straight line and the forehead of the HPM impacted the ground, as shown in Fig. 9e. We conducted two HFOG experiments starting at the heights of 0.6 m and 1 m

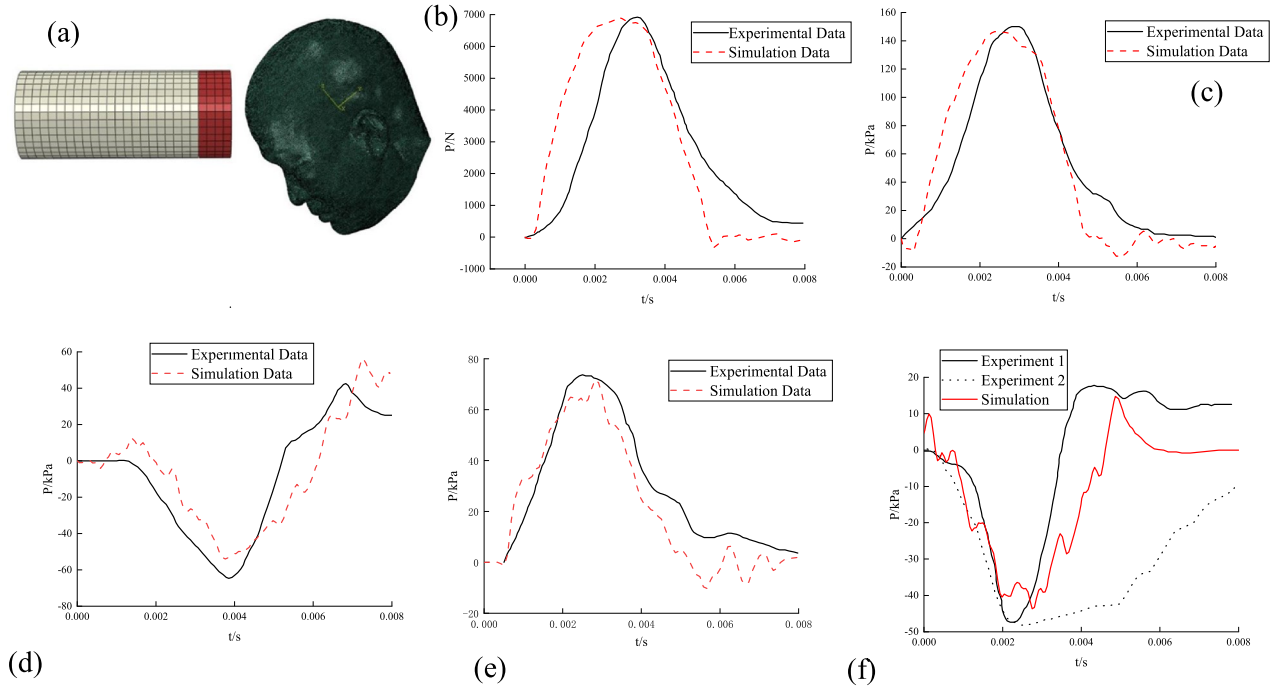

Fig. 3. Comparison of the cadaver test data (Nahum et al.) with the head FE model simulation results: (**a**) simulation of the head crash experiment, (**b**) contact force comparison, (**c**) impact side pressure comparison, (**d**) offset side pressure comparison, (**e**) parietal bone pressure comparison and (**f**) occipital pressure comparison.

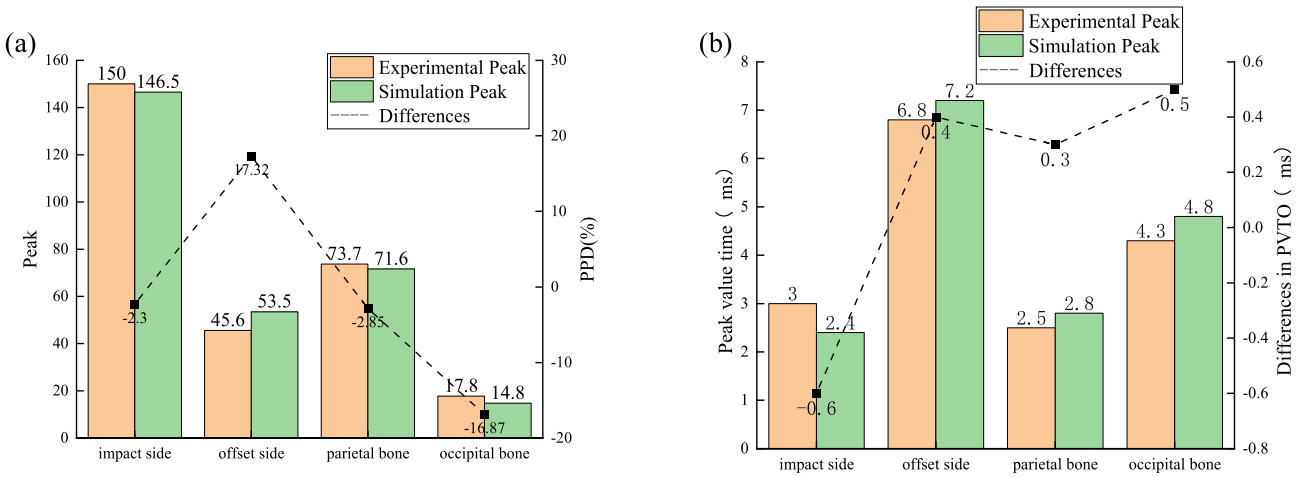

Fig. 4. Analysis of the differences in the intracranial response between the cadaver test data and simulation results: (**a**) PPD of the simulation and experiment, (**b**) the difference in the PVTO of the simulation and experiment.

above the ground. The HPM was placed in an environment at a temperature of 21. 3–23. 2 °C and a humidity of 59–69% for more than 4 h prior to the start of each test. When the HPM fell to the ground, the data acquisition instrument acquired the acceleration in real time and carried out the filtering process (see the black line in Fig. 6). Hence, the kinematic equations for the HPM in free-fall motion are as follows.

$$h = \frac{1}{2}gt^2 \tag{7}$$

where h is the free-fall height and g is the acceleration of gravity; generally, g is set to 9.8 m/s^2, and t is the falling time.

Fig. 5. Simulation settings based on the Yoganandan's experiment.

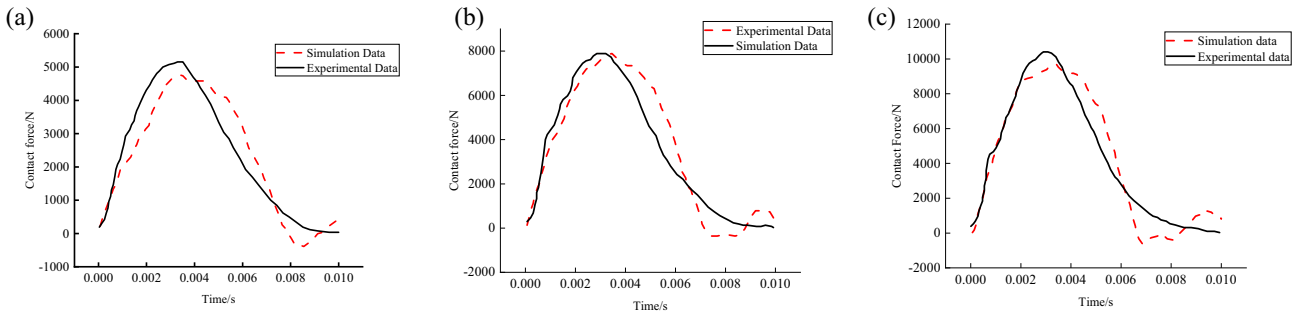

Fig. 6. Comparison of the simulation results of the contact force experiment at different speeds. (**a**) $v = 3.5$ m/s (**b**) $v = 4.9$ m/s and (**c**) $v = 6$ m/s.

Components	E (MPa)	ν	ρ (kg/m^3)	λ (m℃)	αl (10^{-5}/℃)
Surface	27,000	0.15	2500	1.5	1
Foundation course		0.3	2200	1.02	0.6
Soil horizon	30	0.4	1800	0.98	0.45

Table 4. Material parameters of the ground. E: elastic modulus; ν: Poisson's ratio; ρ: density; λ: thermal conductivity; αl: coefficient of linear expansion.

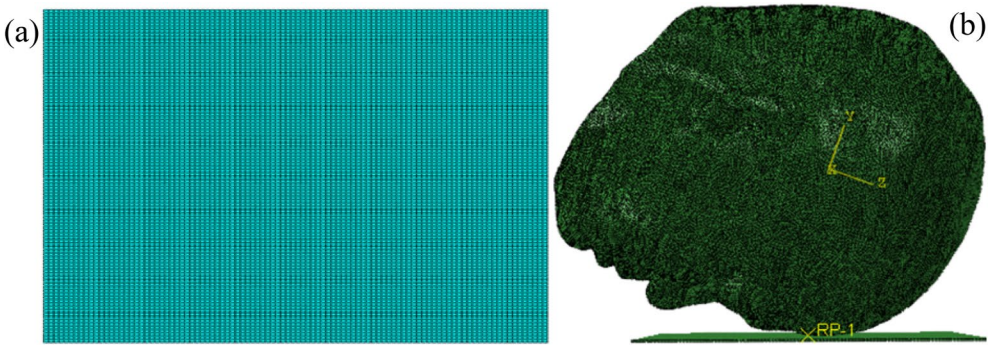

Fig. 7. Construction of the HGC simulation model based on the head FE model: (**a**) FE ground model and (**b**) HGC simulation model.

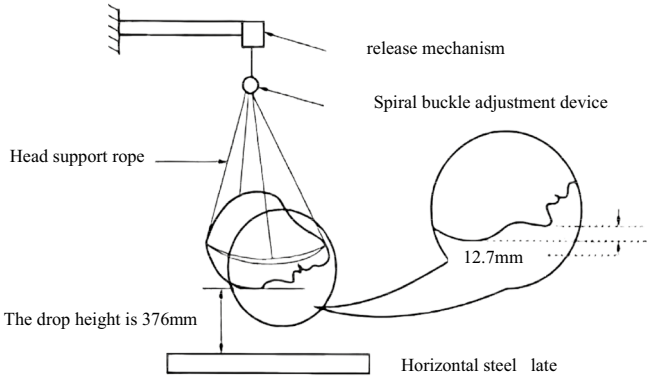

Fig. 8. Schematic diagram of head suspension in Calibration Specification for the Anthropomorphic Test Device of Vehicle Frontal Impact Test (JJF 1803-2020) Chinese standard.

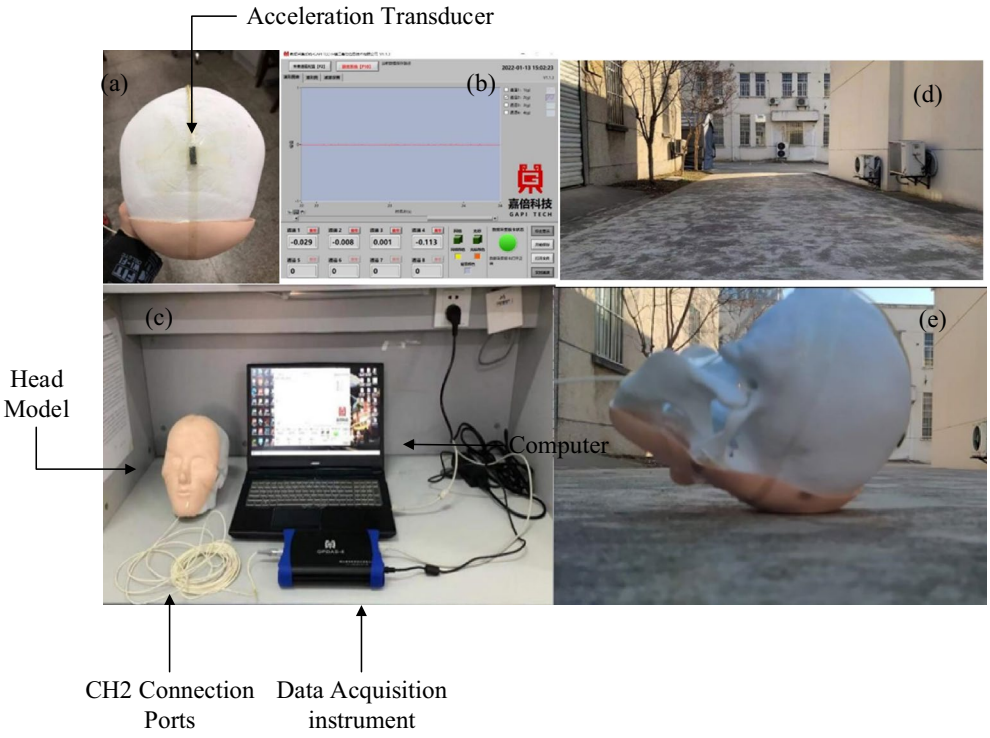

Fig. 9. Photograph showing the materials and process of the head-fall-to-ground experiment: (**a**) fixed acceleration sensor, (**b**) data acquisition system _GAPI_TECH, (**c**) connection of the experimental equipment, (**d**) test scenario and (**e**) after the HPM fell.

$$V = v_0 + gt \tag{8}$$

where V is the HGC velocity, v_0 is the initial speed, and in this study $v_0 = 0$ km/h. Therefore, when h is 0.6 m, V is 12.6 km/h, and when h is 1 m, V is 16.2 km/h.

HGC simulation model validation

To verify the HGC simulation model, we compared the head acceleration data from the HFOG experiment and the HGC simulation model. We set the impact speeds of the HGC simulation model to 12.6 km/h and 16.2 km/h. The simulation time was set to 5 ms. Then, we obtained the acceleration of the FE head model (see the red dashed lines in Fig. 10).

Figure 10 compares the head acceleration curves of the HFOG experiments and HGC simulations. The acceleration curves of the simulation and experiment are in good agreement. When the HGC velocities were 12.6 km/h and 16.2 km/h, the differences in the PVTO were 0.1 ms and – 0.1 ms, and the PPDs were – 6.18% and

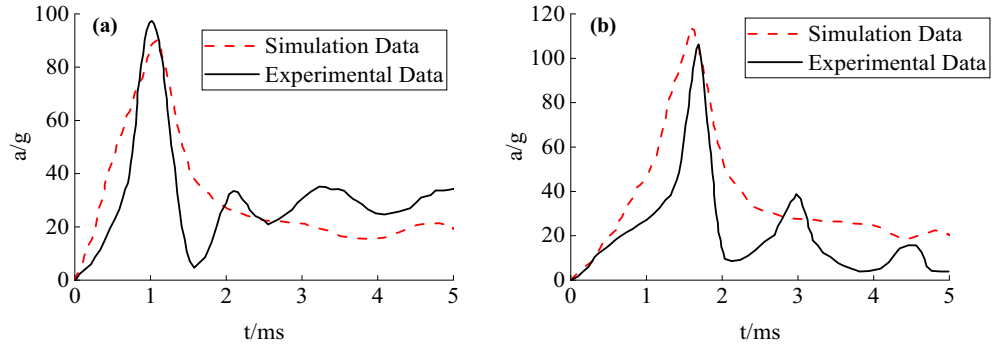

Fig. 10. Experimental and simulated acceleration data plotted versus time for the head falling at different HGC velocities: (**a**) Data for the HGV velocity of 12.6 km/h, (**b**) Data for the HGV velocity of 16.2 km/h.

Regression	Coefficient			Adjust R^2	RMSE
	V^2	V	Constant		
ICP_{LM} ($p<0.05$)	–	12.215 ($p<0.05$)	94.363 ($p<0.05$)	0.954	29.989
ICP_{QM} ($p<0.05$)	0.220 ($p<0.05$)	2.721 ($p>0.05$)	17.939 ($p>0.05$)	0.984	17.819
CR_{LM} ($p<0.05$)	–	2.391 ($p<0.05$)	− 13.172 ($p<0.05$)	0.976	4.189
CR_{QM} ($p<0.05$)	0.033 ($p<0.05$)	0.975 ($p<0.05$)	− 1.770 ($p>0.05$)	0.994	2.111
BS_{LM} ($p<0.05$)	–	1.412 ($p<0.05$)	− 6.320 ($p<0.05$)	0.990	1.596
BS_{QM} ($p<0.05$)	0.011 ($p<0.05$)	0.959 ($p<0.05$)	− 2.668 ($p>0.05$)	0.995	1.116
CL_{LM} ($p<0.05$)	–	2.218 ($p<0.05$)	− 7.597 ($p<0.05$)	0.999	0.855
CL_{QM} ($p<0.05$)	0.006 ($p<0.05$)	1.943 ($p<0.05$)	− 5.384 ($p<0.05$)	1.000	0.491

Table 5. Regression analyses of the relationships between the HGC velocity and brain injury parameters. ICP_{LM}: linear model of the ICP; ICP_{QM}: quadratic model of the ICP; CR_{LM}: linear model of the cerebrum; CR_{QM}: quadratic model of the cerebrum; BS_{LM}: linear model of the brainstem; BS_{QM}: quadratic model of the brainstem; CL_{LM}: linear model of the cerebellum; CL_{QM}: quadratic model of the cerebellum.

5.6%, respectively. Due to the small values of the difference, it is reasonable to conclude that the HGC simulation model accurately reflects the collision conditions.

Regression analysis of pedestrian head injury

Relationship between HGC velocity and head injuries

We examined the relationships between the HGC velocity and brain injury parameters to improve the efficacy of prediction of the degree of head injury. In this study, brain injury parameters included ICP and stress in brain tissues[14]. The different ICPs and stresses in brain-tissue at different HGC velocities (21 datasets) were obtained using the HGC simulation model in the ABAQUS software. We entered these data into SPSS 12 (www.ibm.com/analytics/spss, IBM Inc., USA) to generate the regression models.

The ICP, and the stress of the three main brain tissues (the cerebrum, brainstem, and cerebellum) were selected as the dependent variables, denoted by P_0, σ_{DN}, σ_{NG}, and σ_{XN}. The HGC velocity was the independent variable, denoted by V. Linear and quadratic models were selected for regression analysis.

Table 5 presents the regression results obtained. The R^2 values were above 0.95 for all linear and quadratic models. These findings indicate that the various models have a high degree of fitting. However, for the ICP, V and the constant in the quadratic model were not statistically significant at the 5% significance level. Hence, we choose the linear regression model to reflect the relationship between V and ICP (see Eq. (9)). For cerebral and brainstem stress, some of the parameters in the quadratic models passed the significance test. Therefore, we choose the linear model to describe the relationships between V and stress in the cerebrum and brainstem (see Eqs. (10) and (11)). For cerebellum stress, all of the parameters of the quadratic models were statistically significant, and the RMSE of the quadratic model was smaller than that of the linear model. Hence, the quadratic model is used to describe the relationship between V and cerebellar stress (see Eq. (12)).

$$\hat{P}_0 = 12.215V - 94.363 \tag{9}$$

$$\hat{\sigma}_{DN} = 2.391V - 13.172 \tag{10}$$

$$\hat{\sigma}_{NG} = 1.412V - 6.32 \tag{11}$$

$$\hat{\sigma}_{XN} = 0.006V^2 + 1.943V - 5.384 \tag{12}$$

where $\hat{P}_0$, $\hat{\sigma}_{DN}$, $\hat{\sigma}_{NG}$ and $\hat{\sigma}_{XN}$ are the estimated values of P_0, σ_{DN}, σ_{NG}, and σ_{XN} respectively. According to Eq. (9), when $V \leq 8$ km/h, $\hat{P}_0$ is close to 0, which has little effect on human head injury. According to Eqs. (10)–(12), $\hat{\sigma}_{DN}$, $\hat{\sigma}_{NG}$ and $\hat{\sigma}_{XN}$ are all close to 0, when $V \leq 5$ km/h, which means that in this case, the HGC velocity does not affect human head injury.

Figure 11 shows the relationships between the HGC velocity and P_0, σ_{DN}, σ_{NG}, and σ_{XN}. In Fig. 11, the black dots represent sample points, the red lines represent linear regression, and the blue lines represent quadratic regression. Figure 11 shows that as the velocity of HGC increases, the ICP and the stress in the cerebrum, brainstem, and cerebellum all increase. In particular, the stress growth of the ICP is relatively fast, the stress growth of the brainstem is relatively slow, and the growth trends of the stress of the cerebrum and cerebellum are very close. For a given HGC velocity, the stress on the brainstem is the smallest. Therefore, in subsequent analyses, the injury risk of injury to the ICP, cerebrum, and cerebellum should prioritized when determining whether head injury is life-threatening.

Cutoff value of HGC velocity

It was reported that life-threatening damage to brain tissues can occur when the ICP exceeds 235 kPa[29] or when the stress in the brain tissues exceeds 38 kPa[2]. To obtain a cutoff value of the HGC velocity for the ICP, we substituted the life-threatening ICP (that is, 235 kPa) for $\hat{P}_0$ into Eq. (9), and the corresponding HGC velocity was calculated to be 26.96 km/h. Similarly, we substituted the life-threatening stress of brain tissues (38 kPa) for $\hat{\sigma}_{DN}$, $\hat{\sigma}_{NG}$ and $\hat{\sigma}_{XN}$ in Eqs. (10)–(12), and the corresponding HGC velocities were calculated to be 21.4, 31.39, and 20.97 km/h, respectively. Since 20.97 km is the smallest value among these HGC velocities, it is safe to conclude that in traffic accidents, when the HGC velocity exceeds 20.97 km/h, the pedestrian's head will suffer life-threatening injuries. Hence, 20.97 km/h is determined as the cutoff value of the HGC velocity.

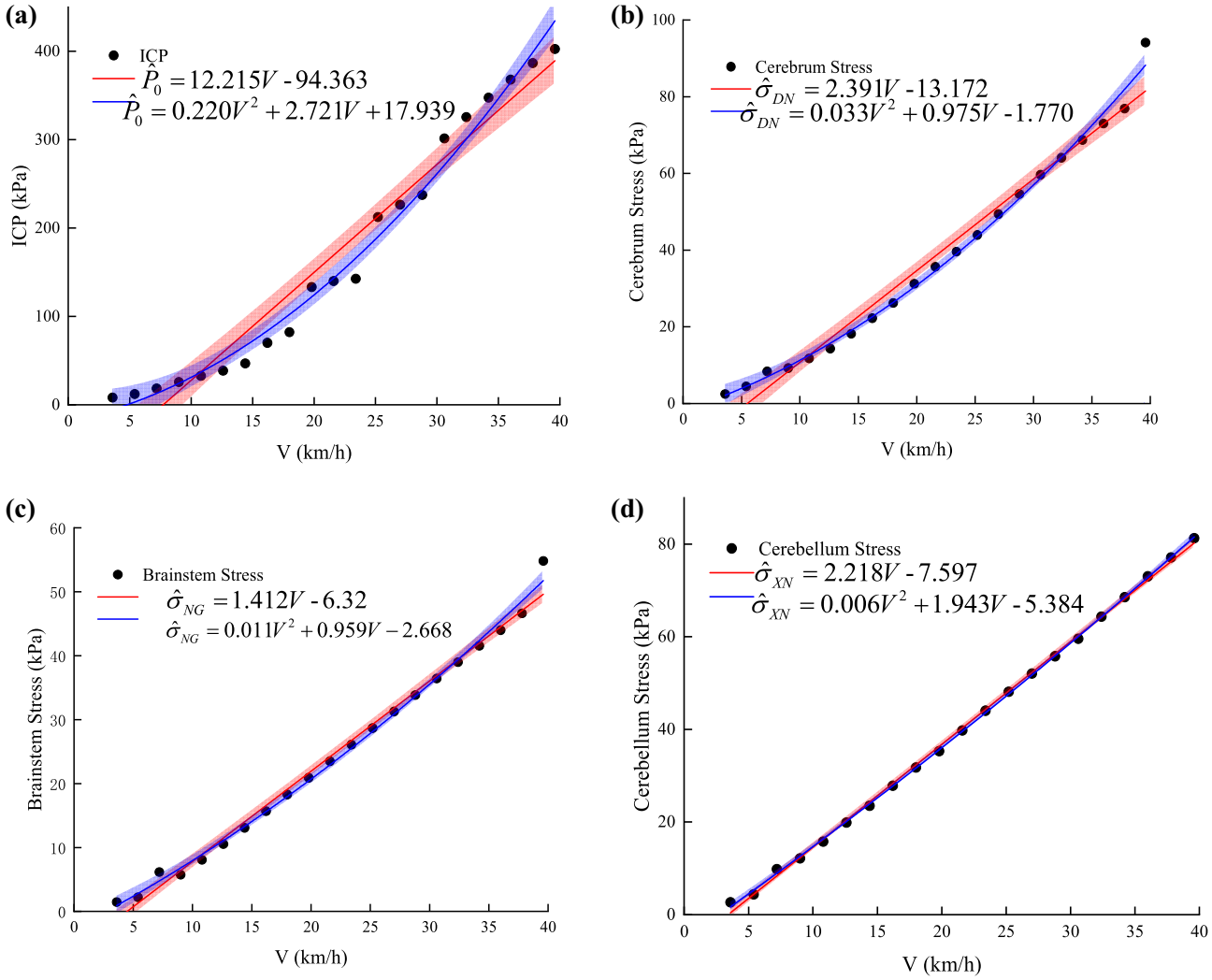

Fig. 11. Regression analysis results (95% confidence intervals) between HGC velocity and intracranial response: (**a**) ICP and HGC velocity, (**b**) cerebral stress and HGC velocity, (**c**) brainstem stress and HGC velocity, (**d**) cerebellar stress and HGC velocity.

Case study

Verification of cutoff value

After constructing the regression models, we examined the reliability of these models by conducting a case study.

The PVC accident used for the case study occurred in Lishui City, Zhejiang Province, China, in 2018. A white Buick four-door car was driving on a dry road. According to the surveillance footage, the driver was driving in the second lane of the road. When the car was driving to the crosswalk, the front right side of the vehicle impacted the pedestrian's left side. Then, the pedestrian fell to the ground and was injured in the head. The pedestrian was taken to the hospital and treated for head trauma, which was not life-threatening. Figure 12a represents the scene of the PVC accident.

We used the PC-Crash (https://www.pc-crash.com/) software to reproduce this traffic accident and obtain the HGC velocity. The Hybrid III dummy model in PC-Crash was used as the pedestrian model. To better represent the pedestrians in the accident, this study modified the corresponding settings according to the basic physical parameters of the Chinese human body[30]. Moreover, the Buick-Regal model in PC-Crash was used as the accident vehicle. The driver's reaction time was set to 1 s, the vehicle body rebound coefficient was set to 0.1, and the road adhesion coefficient was 0.8[31]. After multiple collision simulations in PC-Crash, the trajectory obtained when the velocity of the PVC was 45 km/h was closest to the scene situation. Consequently, Fig. 12b shows the reconstruction accident scene in PC-Crash.

The accident reconstruction results revealed that the back of the pedestrian's head hit the ground when he fell (see Fig. 12c), and the HGC velocity was 14.38 km/h. This value does not exceed the HGC speed cutoff value. This finding is consistent with the findings for the actual accident that the brain trauma of the pedestrian was not life-threatening.

Verification of the regression model

We set the HGC velocity to 14.38 km/h, and the occipital was in the head-ground contact position. Figure 13a shows the head-impact-ground simulation using the validated HGC simulation model.

Figure 13b–e show the ICP and stress propagation in brain tissues. The ICP, cerebral stress, brainstem stress, and cerebellar stress were obtained by collision simulations. We obtained $P_0 = 78.92$ kPa, $\sigma_{DN} = 21.26$ kPa, $\sigma_{NG} = 15.12$ kPa, and $\sigma_{XN} = 26.15$ kPa.

Simultaneously, we substituted the HGC velocity obtained in using PC-Crash (crashed 14.38 km/h) for V into Eqs. (9)–(12), to was easily determine the corresponding ICP and cerebral stress. We obtained $\hat{P}_0 = 81.29$ kPa, $\hat{\sigma}_{DN} = 21.21$ kPa, $\hat{\sigma}_{NG} = 13.98$ kPa and $\hat{\sigma}_{XN} = 23.8$ kPa.

Figure 14 shows a comparison of the PPDs obtained from the simulation (P_0, σ_{DN}, σ_{NG}, σ_{XN}) and from regression models ($\hat{P}_0$, $\hat{\sigma}_{DN}$, $\hat{\sigma}_{NG}$, $\hat{\sigma}_{XN}$). The PPDs of the ICP, cerebrum stress, brainstem stress, and cerebellum stress were − 2.92%, 0.24%, 8.15%, and 9.87%, respectively. These PPDs were within 10%.

The results show that the difference is within an acceptable range, indicating that the regression model can accurately predict the injury of each part of the pedestrian head in a PVC accident.

Verification of multiple traffic cases

To verify the reliability and accuracy of the regression model under different accident circumstances, we collect data on VVC accidents in China. Detailed information, including vehicle information, accident scene information, pedestrian information, and injury records is available about these accidents. Some of the recorded data of these cases are shown in Table 6.

We use PC-Crash to reconstruct these accidents and obtain the corresponding HGC velocities. Next, we substitute these HGC velocities for V in Eqs. (9)–(12). The corresponding ICP and the pressure exerted on the three main brain tissues (i.e., brain, brainstem, and cerebellum) were subsequently obtained, as shown in Table 7. The second column of Table 7 represents the head ground velocity (HGV) obtained from the simulation, and the last column indicates whether it exceeds the injury threshold. Comparing the last column of Table 6 with the last column of Table 7, we find that the proposed formula can provide an efficient and accurate preliminary determination of the severity of the pedestrian injuries.

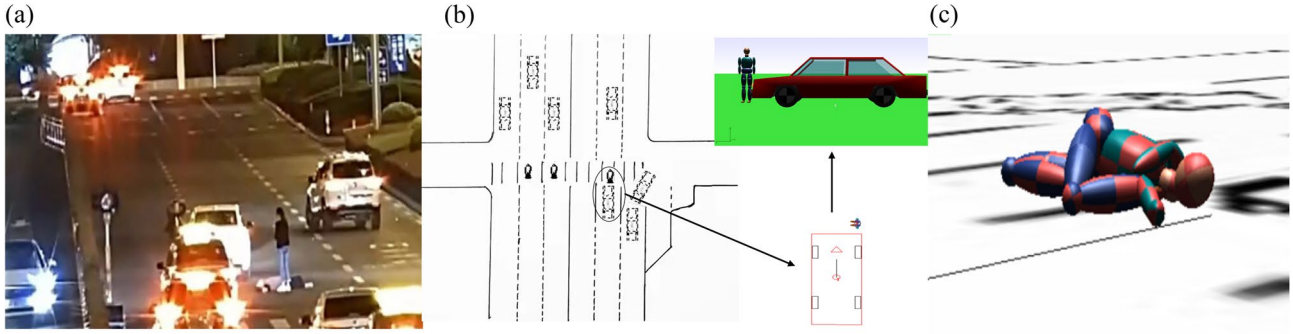

Fig. 12. PVC reconstruction based on real accident cases: (**a**) Scene of the PVC accident, (**b**) PVC accident reconstruction in PC-Crash, (**c**) reproduced pedestrian HGC scene in PC-Crash.

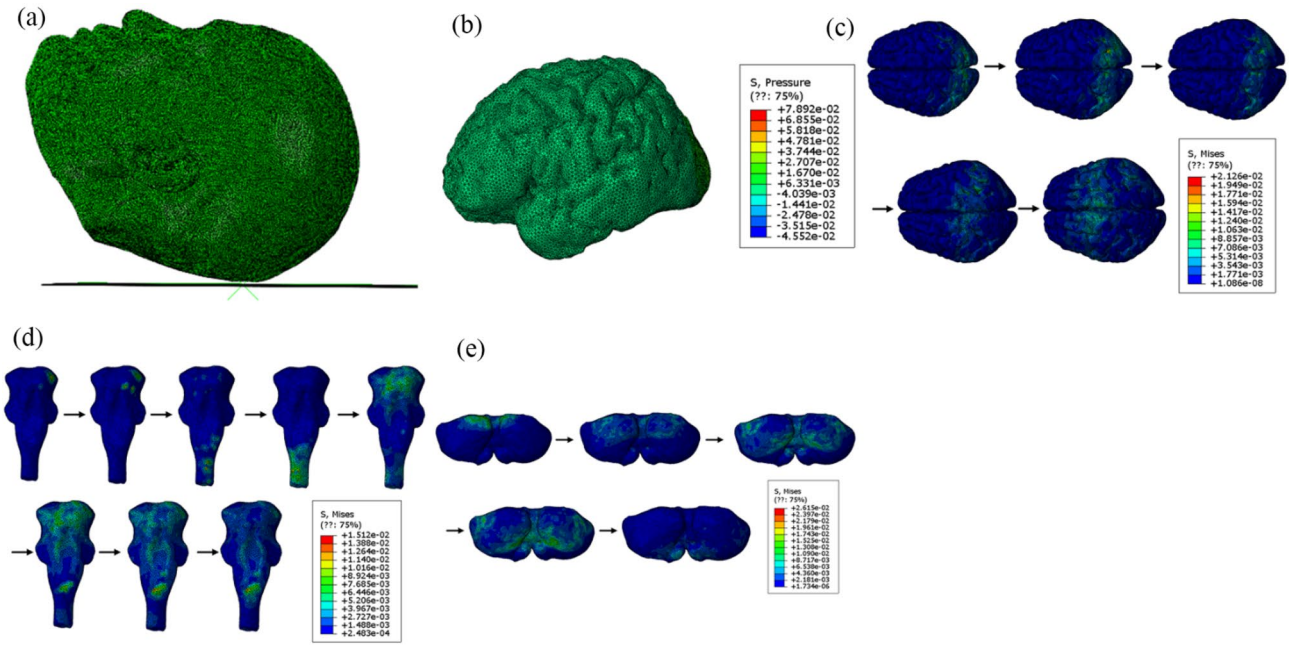

Fig. 13. Analysis of intracranial response results of PVC reconstruction: (**a**) Simulated collision model of HFOG in accident reconstruction, (**b**) ICP in the head FE model, (**c**) cerebrum stress propagation, (**d**) brainstem stress propagation, and (**e**) cerebellum stress propagation.

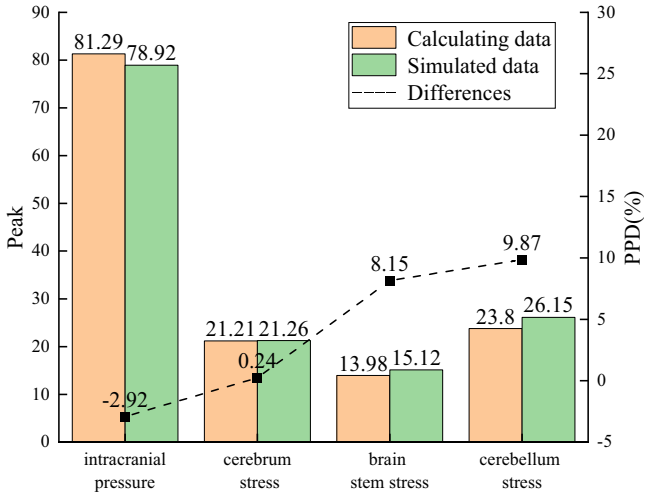

Fig. 14. PPD between the values calculated using the equations obtained from regression analysis and accident reconstruction results.

Conclusions

Regression models for the relationships between the HGC velocity and the ICP and the stress of brain tissues were constructed to explore the degree of brain tissue in the PVC. For each injury index, the cut-off value of the HGC velocity for determining whether the head injury was life-threatening was obtained. This represents an improvement on the existing finite-element-based head injury prediction method, which seldom presents quantitative models and is usually based on FE models that do not use Chinese human attributes or do not provide a detailed description of brain tissues.

This study first constructed and verified an FE head model on the basis of head CT and MRI data from a Chinese 50th-percentile adult male. Next, the HGC simulation model, which consists of the FE head and ground model was established. Its validity was verified using the HFOG experiment of the head physical model. A regression model for the ICP and stress of brain tissues in terms of the HGC velocity was subsequently established, and the cutoff value of velocity was obtained. Based on the actual PVC case study results, we found that the regression model accurately predicts the damage to various parts of the pedestrian's head.

Number	Velocity (km/h)	Vehicle information		Collision location	VRU information		Result
		Brand	Type		Height (cm)	Weight (kg)	Injury severity
1	65	Octavia	Sedan	Left	170	60	Fatal
2	59.87	BMW	Sedan	Left	179	70	Fatal
3	54	Chery	Sedan	right	167	58	Fatal
4	63	Honda	Sedan	Left	170	62	Fatal
5	43	Land-Rover	SUV	front	183	75	Medium
6	61	Changan	SUV	right	162	60	Fatal
7	58	Audi	Sedan	right	165	60	Fatal
8	56	Zotye	SUV	right	170	65	Fatal

Table 6. Actual accident records.

Number	HGV	$\hat{P}_0$	$\hat{\sigma}_{DN}$	$\hat{\sigma}_{NG}$	$\hat{\sigma}_{XN}$	Whether exceed the cut-off value
1	32.11	297.86	63.6	39.02	118.87	Yes
2	31.11	285.65	61.21	37.61	113.13	Yes
3	23.68	194.89	43.45	27.12	74.27	Yes
4	28.96	259.38	56.07	34.57	101.21	Yes
5	19.99	149.81	34.62	21.91	57.43	No
6	32.34	300.67	64.15	39.34	120.21	Yes
7	27.15	237.27	51.74	32.02	91.06	Yes
8	30.55	278.81	59.87	36.82	109.97	Yes

Table 7. Results corresponding to actual accident records.

However, several limitations still need to be addressed. First, other body sizes, such as those of large males and small females, need to be examined in further research. However, since the geometry variations of the head are small relative to those of the other parts of the body, our research results may still be useful to some extent. Second, more detailed information about PVC accidents needs to be collected to enhance the effectiveness and accuracy of the regression models. Third, the relationship between the HGC velocity and PVC velocity should be determined. However, this problem is much more complex because of the many factors affect the relationship between the HGC velocity and PVC velocity, such as pedestrian gait, impact position, and angle.

Data availability

The datasets used and/or analysed during the current study available from the corresponding author on reasonable request.

Received: 23 August 2024; Accepted: 7 May 2025
Published online: 21 May 2025

References

1. WHO. Global status report on road safety 2018. Summary (2018).
2. WHO (ED). International Statistical Classification of Diseases and related health problems Alphabetical index. Geneva (2004).
3. Chen, F. et al. Analysis of craniocerebral injury in facial collision accidents. *PLoS ONE* **15**(10), e0240359 (2020).
4. Nogayeva, S., Gooch, J. & Frascione, N. The forensic investigation of vehicle–pedestrian collisions: A review. *Sci. Justice* **61**(2), 112–118 (2021).
5. Shi, L. et al. Analysis of pedestrian-to-ground impact injury risk in vehicle-to-pedestrian collisions based on rotation angles. *J. Saf. Res.* **64**, 37–47 (2018).
6. Liu, W. et al. Exploration of pedestrian head injuries—collision parameter relationships through a combination of retrospective analysis and finite element method. *Int. J. Environ. Res. Public Health* **13**(12), 1250 (2016).
7. Shi, L. et al. Effects of vehicle front-end safety countermeasures on pedestrian head injury risk during ground impact. *Proc. Inst. Mech. Eng. Part D J. Automob. Eng.* **233**(14), 3588–3599 (2019).
8. Zou, T., Shang, S. & Simms, C. Potential benefits of controlled vehicle braking to reduce pedestrian ground contact injuries. *Accid. Anal. Prev.* **129**, 94–107 (2019).
9. Lv, X. et al. On safety design of vehicle for protection of vulnerable road users: A review. *Thin-Walled Struct.* **182**, 109990 (2023).
10. Fernandes, F. A. O. & de Sousa, R. J. A. Finite element analysis of helmeted oblique impacts and head injury evaluation with a commercial road helmet. *Struct. Eng. Mech.* **48**(5), 661–679 (2013).
11. Wang, X., Peng, Y. & Yi, S. Comparative analyses of bicyclists and motorcyclists in vehicle collisions focusing on head impact responses. *Proc. Inst. Mech. Eng. Part H J. Eng. Med.* **231**(11), 997–1011 (2017).
12. Nasim, M., Cernicchi, A. & Galvanetto, U. Development of a finite element neck model for head-first compressive impacts: Toward the assessment of motorcycle neck protective equipment. *Proc. Inst. Mech. Eng. Part H J. Eng. Med.* **235**(9), 1001–1013 (2021).
13. Xu, J. et al. Do blast induced skull flexures result in axonal deformation?. *PLoS ONE* **13**(3), e0190881 (2018).
14. Marjoux, D. et al. Head injury prediction capability of the HIC, HIP, SIMon and ULP criteria. *Accid. Anal. Prev.* **40**(3), 1135–1148 (2008).

15. Fredriksson, R., Shin, J. & Untaroiu, C. D. Potential of pedestrian protection systems—A parameter study using finite element models of pedestrian dummy and generic passenger vehicles. *Traffic Inj. Prev.* **12**(4), 398–411 (2011).
16. Tamura, A., Koide, T. & Yang, K. H. Effects of translational and rotational accelerations on traumatic brain injury in a sport utility vehicle-to-pedestrian crash. *Int. J. Veh. Des.* **72**, 208 (2016).
17. Wei, W. et al. Head-ground impact conditions and helmet performance in E-scooter falls. *Accid. Anal. Prev.* **181**, 106935 (2023).
18. van Slagmaat, M. et al. Suitability of enhanced head injury criteria for vehicle rating. *Traffic Inj. Prev.* **20**(sup2), S189–S192 (2019).
19. Liu, Q., Wu, X. & Tong, N. Assessment and prediction of acute subdural hematomas in vehicle collision accidents. *Int. J. Crashworthiness* **27**(5), 1444–1459 (2021).
20. Nakadate, H. et al. Finite element head model simulation of the case suspected of diffuse axonal injury in the traffic accident. *Int. J. Crashworthiness* **23**(2), 182–192 (2017).
21. Shi, L. et al. Evaluation of injury thresholds for predicting severe head injuries in vulnerable road users resulting from ground impact via detailed accident reconstructions. *Biomech. Model Mechanobiol.* **19**(5), 1845–1863 (2020).
22. Iwamoto, M., Nakahira, Y. & Kimpara, H. Development and Validation of the Total HUman Model for Safety (THUMS) toward further understanding of occupant injury mechanisms in precrash and during crash. *Traffic Inj. Prev.* **16**(sup1), S36–S48 (2015).
23. Cao, L. et al. Comparison of current ATDs with Chinese adults in anthropometry. *Traffic Inj. Prev.* **17**(4), 430–433 (2015).
24. Zhang, J., Yang, J., Jin, X., Shen, M., Luo, X. & Ma, C. Differences of anthropometric dimensions between Chinese and American and the effects on drivers' injury risks in vehicle frontal crash. *J Automotive Saf. Energy* (2016).
25. Alan, M., Nahum, R. S. & Carley, C. WARD Intracranial pressure dynamics during head impact. In *Proceeding of 21st Stapp Car Crash Conference* (1977).
26. Wang, Q. Construction of the head finite element model and craniocerebral injury in facial collision accident. *Mechanics* **25**(3), 231–239 (2019).
27. Yoganandan, N., Zhang, J. & Pintar, F. A. Force and acceleration corridors from lateral head impact. *Traffic Inj. Prev.* **5**(4), 368–373 (2010).
28. Hodgson, V., Mason, M. & Thomas, L. Head model for impact. SAE Technical Paper (1972).
29. Avalle, M., Belingardi, G. & Ibba, A. Mechanical models of cellular solids Parameters identification from experimental tests. *Int. J. Impact. Eng.* **34**, 3–27 (2007).
30. Reed, R. A. et al. Physical processes and applications of the Monte Carlo Radiative Energy Deposition (MRED) code. *IEEE Trans. Nucl. Sci.* **62**(4), 1441–1461 (2015).
31. Viikari, V. V., Varpula, T. & Kantanen, M. Road-condition recognition using 24-GHz automotive radar. *IEEE Trans. Intell. Transp. Syst.* **10**(4), 639–648 (2009).

Author contributions

Y.L.: Conceptualization, Methodology, Writing—review & editing, Modification. J.B.: Wrote the main manuscript text and prepared figures and tables. Y.L.: Wrote the main manuscript text and prepared figures and tables. Y.S.: Provide research data and review manuscripts.

Funding

This work was supported by the National Natural Science Foundation of China (No. 51605197), the Natural Science Foundation of Jiangsu Province (No. BK20160524); the National Key Research and Development Program (No. 2019YFB1600500); the Key Research and Development Plan of Zhenjiang City (No. SH2019054).

Declarations

Competing interests

The authors declare no competing interests.

Additional information

Correspondence and requests for materials should be addressed to Y.L.